# Interplay between band crossing and charge density wave instabilities

P. Grigoriev, A. Sinchenko, P. Vorobyev, A. Hadj-Azzem, P. Lejay, A. Bosak, P. Monceau

Rapid Communications

# Interplay between band crossing and charge density wave instabilities

P. D. Grigoriev,[1,2,3] A. A. Sinchenko,[4,5] P. A. Vorobyev,[4] A. Hadj-Azzem,[6] P. Lejay,[6] A. Bosak,[7] and P. Monceau[6]

[1]*L. D. Landau Institute for Theoretical Physics, 142432 Chernogolovka, Russia*
[2]*National University of Science and Technology "MISiS," 119049 Moscow, Russia*
[3]*P. N. Lebedev Physical Institute, RAS, 119991 Moscow, Russia*
[4]*M. V. Lomonosov Moscow State University, 119991 Moscow, Russia*
[5]*Kotelnikov Institute of Radioengineering and Electronics of RAS, 125009 Moscow, Russia*
[6]*Université Grenoble Alpes, CNRS, Institut Néel, F-38042 Grenoble, France*
[7]*ESRF - The European Synchrotron, 71, Avenue des Martyrs, F-38000 Grenoble, France*

(Received 6 February 2019; revised manuscript received 2 August 2019; published 22 August 2019)

Our measurements of the Hall coefficient in rare-earth tritelluride compounds reveal a strong hysteresis between cooling and warming in the low-temperature range where a second unidirectional charge density wave (CDW) occurs. We show that this effect results from the interplay between two instabilities: band crossing of the Te $p_x$ and $p_y$ orbitals at the Fermi level and CDW, which have a close energy gain and compete. Calculation of the electron susceptibility at the CDW wave vector with and without band anticrossing reconstruction of the electron spectrum yields a satisfactory estimation of the temperature range of the hysteresis in Hall effect measurements.

DOI: 10.1103/PhysRevB.100.081109

Crossing of electron energy bands near the Fermi level, resulting in the degeneracy and anticrossing of energy levels, always leads to amazing physical properties. The anticrossing of spin-split energy bands with spin-orbit coupling produces nontrivial topologically protected electron states in Weyl and Dirac semimetals, which has been the subject of extensive research for the last decade [1–4]. Even without spin effects, the band anticrossing near the Fermi level modifies the electron spectrum and the Fermi surface (FS). This affects various electronic instabilities such as superconductivity in high-temperature cuprate superconductors [5–7] and spin or charge density waves [8–10]. In this Rapid Communication we unveil the competition of band anticrossing and the charge density wave (CDW) in the family of rare-earth tritelluride compounds. We show, both theoretically and experimentally, that this interplay leads to a hysteretic electronic phase transition with the change of FS topology and of the Hall coefficient.

Layered compounds of the $R\mathrm{Te}_3$ family ($R$ = rare-earth atom) have a weakly orthorhombic crystal structure (space group *Cmcm*). These systems exhibit an incommensurate CDW through the whole $R$ series [8,11,12], with a wave vector $\mathbf{Q}_{\mathrm{CDW1}} = (0, 0, \sim 2/7c^*)$ and a Peierls transition temperature above 300 K for the light atoms (La, Ce, Nd). For the heavier $R$ (Tb, Dy, Ho, Er, Tm) a second CDW occurs at low temperature with the wave vector $\mathbf{Q}_{\mathrm{CDW2}} = (\sim 2/7a^*, 0, 0)$ perpendicular to $\mathbf{Q}_{\mathrm{CDW1}}$.

For our study we chose three compounds from the $R\mathrm{Te}_3$ family: two compounds, $\mathrm{ErTe}_3$ and $\mathrm{HoTe}_3$, demonstrating bidirectional CDW ordering at $T_{\mathrm{CDW1}} = 270$ and 283 K and $T_{\mathrm{CDW2}} = 160$ and 110 K correspondingly, and $\mathrm{TbTe}_3$, revealing a unidirectional CDW at $T_{\mathrm{CDW}} = 336$ K. Single crystals of these compounds were grown by a self-flux technique under purified argon atmosphere as described previously [13]. Thin samples with a typical thickness 1–3 $\mu$m having a rectangular shape were prepared by micromechanical exfoliation of relatively thick crystals glued on a sapphire substrate.

The magnetic field was applied parallel to the $b$ axis. The Hall resistance $R_{xy}(B) = [V_{xy}(+B) - V_{xy}(-B)]/I$ was recorded using the van der Pauw method [14,15], sweeping the field between +6 and −6 T at a fixed temperature with a step $\Delta T = 10$ K first by cooling from $T > T_{\mathrm{CDW1}}$ down to 4.2 K and after that by warming back up.

For all measured compounds $R_{xy}$ is a linear function of $B$ at least for temperatures $T \gtrsim 100$ K [16]. So, the Hall constant, $R_H = R_{xy}d/B$, where $d$ is the crystal thickness, is indeed a field-independent quantity. Its temperature dependencies for $\mathrm{ErTe}_3$, $\mathrm{HoTe}_3$, and $\mathrm{TbTe}_3$ are shown in Figs. 1(a)–1(c) correspondingly. One can see that for $\mathrm{ErTe}_3$ and $\mathrm{HoTe}_3$, $R_H$ demonstrates a strong hysteresis between cooling and warming in the temperature range around the second Peierls transition while $R_H(T)$ is completely reversible for $\mathrm{TbTe}_3$, revealing only a single transition to the CDW state in the studied range of temperature. When measured under cooling and warming the temperature dependence of the resistance $R(T)$ of all three compounds was reversible [16]. It means that the total number of charge carriers remains nearly the same under cooling and warming. We see only one explanation for this effect: There are two types of carriers, and the hysteresis observed is attributed to the change in electron-hole balance as a result of the second CDW formation. Such a scenario is confirmed by the change of the sign of the Hall constant at a certain temperature in $\mathrm{HoTe}_3$ and $\mathrm{TbTe}_3$.

One can naturally attribute the observed effect to the hysteresis of the CDW wave vector $\boldsymbol{Q}_{\mathrm{CDW}}$ due to its pinning by crystal imperfections. However, our preliminary x-ray diffraction studies of $\mathrm{ErTe}_3$, performed at ID28 ESRF beamline [17], showed a completely reversible evolution of

 

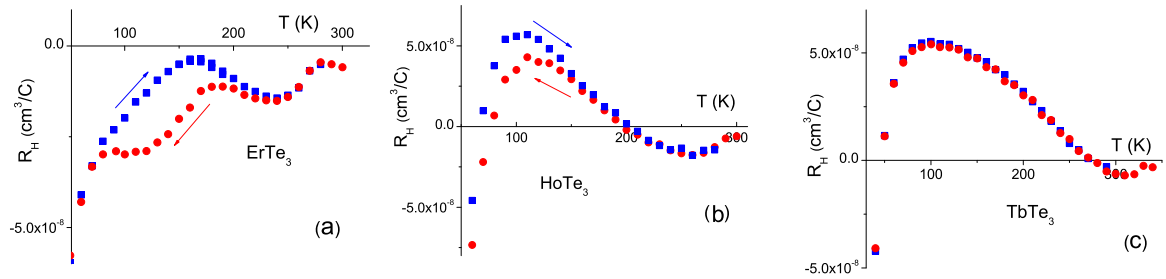


FIG. 1. Hall constant of (a) $ErTe_3$, (b) $HoTe_3$, and (c) $TbTe_3$ as a function of temperature. Red circles correspond to cooling, and blue squares correspond to warming.

all structural parameters in the temperature range 100–300 K [16]. Therefore, we consider another possible origin of this hysteresis, based on the interplay of $CDW_2$ with another type of electronic instability. As a possible candidate for such electronic ordering competing with $CDW_2$, we suggest the one due to the electron band crossing at the Fermi level.

Consider two electron bands with electron dispersion $\epsilon_1(\boldsymbol{k})$ and $\epsilon_2(\boldsymbol{k})$. Two corresponding Fermi surfaces, given by the equations $\epsilon_1(\boldsymbol{k}) = E_F$ and $\epsilon_2(\boldsymbol{k}) = E_F$, intersect along the lines $\{\boldsymbol{k}_0\}$ in the momentum space. In $R\mathrm{Te}_3$ compounds in the $(k_x, k_y)$ plane below $T_{\mathrm{CDW1}}$ there are two such crossing points $\boldsymbol{k}_0$ [18], highlighted by solid yellow circles in Fig. 2. At each degeneracy point $\boldsymbol{k}_0$, any small interband coupling $V(\boldsymbol{Q})$, even at zero momentum transfer $\boldsymbol{Q} = \boldsymbol{0}$, leads to the band anticrossing and to the reconstruction of FS (see the upper right inset in Fig. 2). This FS anticrossing has been observed in various $R\mathrm{Te}_3$ compounds by angle-resolved photoemission spectroscopy (ARPES) measurements [12,19]. The interband coupling $V(\boldsymbol{Q})$ may originate, e.g., from the electron-electron ($e$–$e$) interaction. Usually, $|V(\boldsymbol{Q})|$ decreases with an increase of momentum transfer $|\boldsymbol{Q}|$, and $|V(\boldsymbol{0})| \equiv V_0$ may considerably exceed $|V(\boldsymbol{Q} \neq \boldsymbol{0})|$.

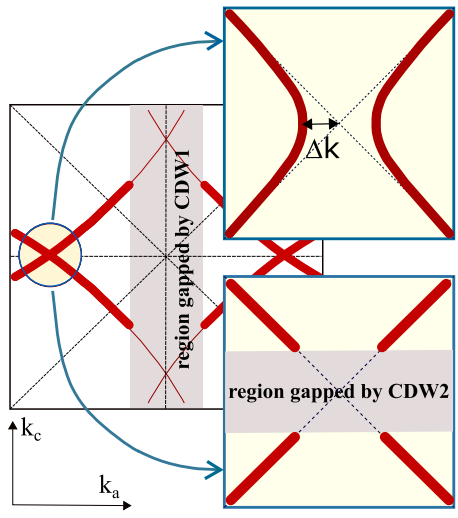


FIG. 2. Schematic representation of the Fermi surface (FS) in $RTe_3$. Main figure: The full FS with the $CDW_1$-gapped region shaded by gray. In the crossing region, highlighted by a solid yellow circle, two FS reconstructions are possible: with band anticrossing shown in the upper right inset, and with an energy gap due to $CDW_2$ shaded by gray in the lower right inset.

First, consider the toy model with the interband coupling (off-diagonal terms) only at $\boldsymbol{Q} = \boldsymbol{0}$. In this model the different momenta are not coupled, and the Hamiltonian writes down as a sum over electron momenta $\boldsymbol{k}$, $\hat{H} = \sum_{\boldsymbol{k}} \hat{H}_{\boldsymbol{k}}$, where in the basis of two branches $\alpha = 1, 2$ of the electron spectrum each term $\hat{H}_{\boldsymbol{k}}$ is given by a $2 \times 2$ matrix [20],

$$\hat{H}_{\boldsymbol{k}} = \begin{pmatrix} \epsilon_1(\boldsymbol{k}) & V_0 \\ V_0 & \epsilon_2(\boldsymbol{k}) \end{pmatrix}, \tag{1}$$

with two eigenvalues,

$$E_{\pm}(\boldsymbol{k}) = \frac{\epsilon_1(\boldsymbol{k}) + \epsilon_2(\boldsymbol{k})}{2} \pm \sqrt{\left(\frac{\epsilon_1(\boldsymbol{k}) - \epsilon_2(\boldsymbol{k})}{2}\right)^2 + V_0^2}, \tag{2}$$

representing two new branches of the electron spectrum. The total electron energy is given by the sum of quasiparticle energies over their quantum numbers,

$$\mathcal{E} = \sum_{\boldsymbol{k},\alpha} E_\alpha(\boldsymbol{k}) n_F[E_\alpha(\boldsymbol{k})], \tag{3}$$

where $n_F(\varepsilon) = 1/(1 + \exp[(\varepsilon - E_F)/T])$ is the Fermi-Dirac distribution function. Without band anticrossing the total energy $\mathcal{E}_0$ is given by the same Eq. (3) with the replacement $E_\alpha(\boldsymbol{k}) \to \epsilon_\alpha(\boldsymbol{k})$. The difference $\Delta\mathcal{E}_{\mathrm{AC}} = \mathcal{E} - \mathcal{E}_0$ comes mainly from the vicinity of the crossing points $\boldsymbol{k}_0$, where two conditions are satisfied: (i) $|\epsilon_1(\boldsymbol{k}) - \epsilon_2(\boldsymbol{k})| \lesssim V_0$, so that the electron spectrum changes considerably, and (ii) $|\epsilon_1(\boldsymbol{k}) + \epsilon_2(\boldsymbol{k})| \lesssim 2V_0$, so that the change in the electron spectrum is close to the Fermi level. Near the crossing point $\boldsymbol{k}_0$ one may linearize each branch of the electron spectrum,

$$\epsilon_\alpha(\boldsymbol{k}) \approx \boldsymbol{v}_{F\alpha}(\boldsymbol{k} - \boldsymbol{k}_0), \tag{4}$$

where $\boldsymbol{v}_{F\alpha}$ is the Fermi velocity $v_F$ of branch $\alpha$. Then $|\epsilon_1(\boldsymbol{k}) \pm \epsilon_2(\boldsymbol{k})| \approx (\boldsymbol{v}_{F1} \pm \boldsymbol{v}_{F1})(\boldsymbol{k} - \boldsymbol{k}_0) \sim v_F|\boldsymbol{k} - \boldsymbol{k}_0|$, and the contributing momentum area in the vicinity of the crossing point $\boldsymbol{k}_0$ is estimated as $(V_0/v_F)^2$. Then the energy difference per unit area per one spin component but including two cross points is

$$\Delta\mathcal{E}_{AC} \sim -(V_0/\pi\hbar v_F)^2 V_0 \approx -V_0^3\, a^2 \rho_F^2, \tag{5}$$

where $a$ is the in-plane lattice constant and $\rho_F = 1/\pi\hbar v_F a$ is the quasi-one-dimensional (1D) density of states (DOS) at the Fermi level per one branch and spin component. Our calculation of $\Delta\mathcal{E}_{\mathrm{AC}}$ by the numerical integration according to Eq. (3) confirms the estimate in Eq. (5), giving a $\Delta\mathcal{E}_{\mathrm{AC}}$ value 20% less than in Eq. (5).

The CDW energy gain per spin component is [21,22]

$$\Delta\mathcal{E}_{\rm CDW} = -\Delta^2\rho_F, \tag{6}$$

where $\Delta$ is the CDW energy gap. The extra small parameter $\eta \equiv V_0\rho_F a^2 = V_0 a/\pi\hbar v_F \ll 1$ in the band crossing energy gain in Eq. (5) as compared to Eq. (6) comes from the small momentum region of contributing electrons, while in a CDW a considerable part of the electrons on the Fermi level participates in the Peierls instability, so that a similar small factor $a^2\rho_F\Delta$ does not appear. Hence, the $CDW_2$ energy gain may be larger than the energy gain from band anticrossing, although its energy gap $\Delta_2 \ll V_0$.

We estimate the value of $V_0$ from the FS distortion at the crossing point $\boldsymbol{k}_0$ observed in ARPES. This FS distortion $\Delta k$ along the $x$ axis is about 3% of the Brillouin zone width $2\pi\hbar/a$ [12,19], where the lattice constant $a = 4.28$ Å in $ErTe_3$. This $\Delta k$ corresponds to the condition $|\epsilon_1(\boldsymbol{k}) + \epsilon_2(\boldsymbol{k})| = 2V_0$, giving the boundary of electron states with a gap on the Fermi level according to Eq. (2). In $R\mathrm{Te}_3$ compounds the FSs of two bands cross at almost a right angle, as shown in Fig. 2. Substituting the electron dispersion (4) with $v_F \approx 1.3\times10^8$ cm/s, we obtain in $ErTe_3$ compounds $V_0 \approx v_F\Delta k/\sqrt{2} \approx 250$ meV. For comparison, in $ErTe_3$ the $CDW_1$ energy gap $\Delta_1 \approx 175$ meV, and the $CDW_2$ energy gap is $\Delta_2 \approx 55$ meV [23]. The parameter $\eta = V_0 a/\pi\hbar v_F \approx 0.04$ is indeed $\ll 1$, and the ratio of energy gains from the band anticrossing and from $CDW_2$ is $\Delta\mathcal{E}_{\rm AC}/\Delta\mathcal{E}_{\rm CDW2} \approx \eta V_0^2/\Delta_2^2 \approx 0.8$, i.e., slightly less than unity. This means a strong temperature-dependent interplay of these two electronic instabilities, making $CDW_2$ slightly more energetically favorable at low $T$. However, since $V_0/\Delta_2 \approx 5 \gg 1$, the band anticrossing appears at a much higher temperature than $T_{\rm CDW2}$, even higher than $T_{\rm CDW1}$.

The band anticrossing and $CDW_2$ hinder each other by changing the electron spectrum. The $CDW_2$ creates an energy gap on the Fermi level just at the spots of FS intersection (see the lower right inset in Fig. 2), thus suppressing or making irrelevant the band anticrossing. The influence of band anticrossing on $CDW_2$ is less obvious, because the FS has an approximate nesting property both with and without the band anticrossing. Moreover, our calculation of the DOS with and without band anticrossing gives nearly the same result in both cases. Hence, to substantiate that band anticrossing hinders the $CDW_2$ instability, we need to compare the electronic susceptibility $\chi(\boldsymbol{Q}, T)$ at the $CDW_2$ wave vector $\boldsymbol{Q}$ in both cases: with and without band anticrossing reconstruction of the electron spectrum. The $CDW_2$ transition temperature $T_c$ is given by the equation [21] $|U\chi(\boldsymbol{Q}_{\max}, T_c)| = 1$, where $\boldsymbol{Q}_{\max}$ is the wave vector where the susceptibility $\chi$ takes a maximum value. The larger the susceptibility $\chi$, the higher is the CDW transition temperature, because susceptibility increases with a decrease of temperature.

For calculations we use the well-known formula for the static susceptibility of free-electron gas at a finite wave vector $\boldsymbol{Q}$. Electron spin only leads to a factor 4 in susceptibility, but the summation over the band index $\alpha$ must be retained. Then the real part of electron susceptibility is

$$\chi(\boldsymbol{Q}) = \sum_{\alpha,\alpha'}\int \frac{4d^d\boldsymbol{k}}{(2\pi)^d}\frac{n_F(E_{\boldsymbol{k},\alpha}) - n_F(E_{\boldsymbol{k}+\boldsymbol{Q},\alpha'})}{E_{\boldsymbol{k}+\boldsymbol{Q},\alpha'} - E_{\boldsymbol{k},\alpha}}, \tag{7}$$

where $d$ is the dimension of space. In $R\mathrm{Te}_3$ compounds under study there are two bands crossing the Fermi level, $\alpha, \alpha' = 1, 2$, and we may take $d = 2$ because the dispersion in the $z$ direction is weak. Equation (7) differs only by the summation over $\alpha$ and $\alpha'$ from the common expression, e.g., given in Eq. (1.7) of Ref. [21].

Taking the tight-binding bare electron dispersion $\epsilon_{1,2}(\boldsymbol{k})$ commonly used [9,24] for $R\mathrm{Te}_3$ compounds and given by Eqs. (2) of Ref. [24], we calculate the susceptibility in Eq. (7) as a function of the wave vector $\boldsymbol{Q}$ and temperature $T$ for two cases: without the band crossing effect, i.e., for bare electron dispersion $\epsilon_{1,2}(\boldsymbol{k})$, and for a reconstructed dispersion given by Eq. (2). The results are shown in Fig. 3. The integration over momentum in Eq. (7) is performed only at $k_x > k_{x0} \approx 0.29$ Å$^{-1}$, because in the momentum region $|k_x| < k_{x0}$ the electron spectrum at the Fermi level has a large energy gap $\Delta_1$ due to $CDW_1$.

The summation over $\alpha$ and $\alpha'$ in Eq. (7) gives four terms: two intraband terms $\chi$ with $\alpha = \alpha'$ and two interband terms $\Delta\chi$ with $\alpha \neq \alpha'$. The intraband "diagonal" terms, enhanced by a rather good FS nesting, are much larger than the "off-diagonal" interband terms, because the latter correspond to almost perpendicular FS sheets and do not have such a nesting

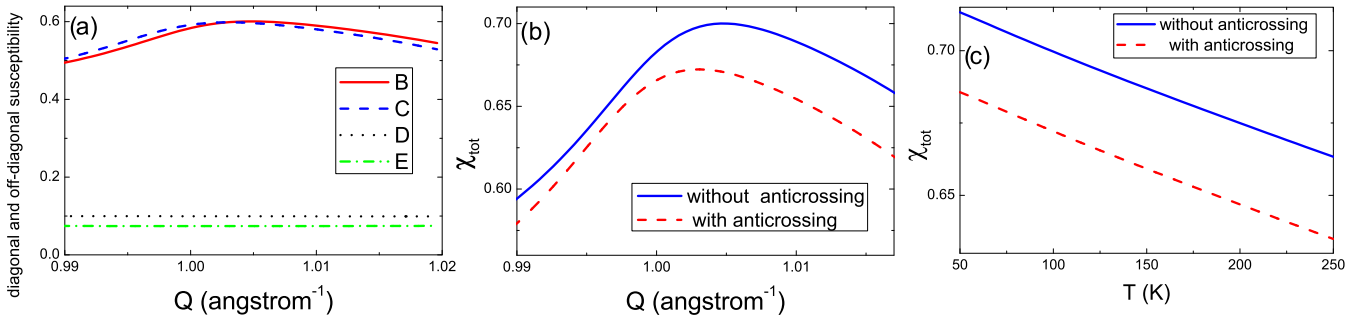


FIG. 3. Calculated electron susceptibility. (a) The electron susceptibility contributions without (solid blue and green lines) and with the band crossing reconstruction (dashed red and black lines). The upper two curves (blue and red) show the calculated "diagonal" intraband contributions $\chi$, while the two lower curves (green and black) show "off-diagonal" interband contributions $\Delta\chi$ to susceptibility. (b) Total susceptibility $\chi_{\rm total} = \chi + \Delta\chi$ as a function of wave vector $Q_x$ near its maximum without (solid blue line) and with the band crossing reconstruction (dashed red line). (c) The temperature dependence of maximal total susceptibility without (solid blue line) and with the band crossing reconstruction (dashed red line).

enhancement [see Fig. 3(a)]. Hence, the intraband contribution, shown by the upper blue and red curves in Fig. 3(a), have a maximum at the $CDW_2$ wave vector $\boldsymbol{Q}$, resulting in a similar maximum on the total susceptibility in Fig. 3(b), while the interband contribution, shown by the lower green and black curves in Fig. 3(a), depends weakly on $\boldsymbol{Q}$. Nevertheless, the interband contribution is considerable, being about 20% of the intraband susceptibility. This again illustrates the well-known fact [25,26] that the Fermi-surface nesting does not determine the CDW properties.

While the maximum values of the diagonal intraband susceptibility terms are weakly affected by the band anticrossing, the off-diagonal interband terms are suppressed by the band anticrossing reconstruction by more than 20% [see Fig. 3(a)]. This can be easily understood by looking at the FS with and without band anticrossing, shown in Fig. 2. The DOS and the nesting property are not violated by the band anticrossing, hence, the intraband terms remain almost the same (only the optimal $CDW_2$ wave vector slightly shifts). On the contrary, after the band anticrossing reconstruction, the FSs of different bands become separated by $\Delta k \sim 3\%$ of the Brillouin zone. Two FS sheets even do not intersect, as was without the band anticrossing. Hence, the interband susceptibility decreases considerably.

We have shown that the band anticrossing and $CDW_2$ interfere, suppressing each other. With a temperature decrease the band anticrossing appears first (at a higher temperature) and reduces the $CDW_2$ transition temperature to its observed value $T_{CDW2}$. At a lower temperature, when $CDW_2$ develops and the $\Delta_2$ increases, since $|\Delta\mathcal{E}_{CDW2}| > |\Delta E_{AC}|$, the band anticrossing shrinks in favor of $CDW_2$. This may happen as a first-order phase transition, accompanied by a hysteresis. When the temperature increases again, the $CDW_2$ disappears at temperature $T^*_{CDW2} > T_{CDW2}$, because of the changed band crossing energy spectrum. This results in a hysteresis seen by the Hall coefficient sensitive to the FS reconstruction due to $CDW_2$. We can estimate how strong this hysteresis is by looking at the calculated temperature dependence of susceptibility $\chi(T)$, shown in Fig. 3(c). The calculated optimal wave vector $\boldsymbol{Q}$ of the $CDW_2$ instability, i.e., of the susceptibility maximum shown in Fig. 3(b), very slightly increases with temperature from $Q_x \approx 1.004$ Å$^{-1}$ at $T = 50$ K to $Q_x \approx 1.006$ Å$^{-1}$ at $T = 200$ K. Therefore, this change was not observed in the x-ray experiment [see the Supplemental Material (SM) [16]]. In Fig. 3(c) we plot the maximum value of $\chi(\boldsymbol{Q})$ as a function of temperature $T$ without (solid blue line) and with (dashed red line) band crossing reconstruction. They differ by 4.5% only, but since the temperature dependence of susceptibility is also quite weak, the susceptibility value $\chi_c = 0.68$, which the red curve reaches only at $T_c \approx 50$ K, the blue curve has already at $T^*_c \approx 175$ K. Thus, the expected temperature hysteresis is rather large: $\Delta T = T^*_c - T_c \approx 125$ K [27].

The proposed interplay between band crossing and CDW is rather general and is expected in many other compounds with a FS intersection at the nested parts. For example, a similar effect is expected in the $R\mathrm{Te}_4$ family of compounds, where a large temperature hysteresis of resistance $\Delta T > 100$ K has also been observed recently [10].

The bilayer splitting of the electron spectrum smears the nesting condition [23]. The exact bare electron dispersions $\epsilon_{1,2}(\boldsymbol{k})$ are unknown. The coupling between two CDWs in the above analysis is taken into account only by neglecting the contribution from the states gapped by $CDW_1$. These and other factors make the interplay of $CDW_2$ with other instabilities more complicated, but we expect that the main features of the proposed model remain valid.

To summarize, we observed a strong hysteresis of the Hall coefficient in the rare-earth tritelluride compounds $ErTe_3$ and $HoTe_3$, having two CDW phase transitions. We explain this effect by a strong interplay of the low-temperature CDW and the band anticrossing change of the electron spectrum. We estimate the temperature range of this hysteresis by calculating the electron susceptibility at the $CDW_2$ wave vector with and without band anticrossing. The interplay between these two instabilities is proposed and investigated and may be relevant to other compounds where two electron bands cross at the Fermi level.

The authors are grateful to the staff of the ID28 beamline ESRF. The work was partially supported by joint grant CNRS and Russian State Fund for the Basic Research (No. 17-52-150007) and by the Foundation for Advancement of Theoretical Physics and Mathematics "BASIS." P.V. thanks RFBR Grant No. 19-02-01000. P.G. thanks State Assignment No. 0033-2019-0001 "The development of condensed-matter theory." A.S. thanks State Assignment IRE RAS.

[1] M. Z. Hasan and C. L. Kane, Rev. Mod. Phys. **82**, 3045 (2010).
[2] X.-L. Qi and S.-C. Zhang, Rev. Mod. Phys. **83**, 1057 (2011).
[3] B. Yan and C. Felser, Annu. Rev. Condens. Matter Phys. **8**, 337 (2017).
[4] N. P. Armitage, E. J. Mele, and A. Vishwanath, Rev. Mod. Phys. **90**, 015001 (2018).
[5] E. Razzoli, C. E. Matt, Y. Sassa, M. Mansson, O. Tjernberg, G. Drachuck, M. Monomo, M. Oda, T. Kurosawa, Y. Huang, N. C. Plumb, M. Radovic, A. Keren, L. Patthey, J. Mesot, and M. Shi, Phys. Rev. B **95**, 224504 (2017).
[6] M. Horio, K. Hauser, Y. Sassa, Z. Mingazheva, D. Sutter, K. Kramer, A. Cook, E. Nocerino, O. K. Forslund, O. Tjernberg, M. Kobayashi, A. Chikina, N. B. M. Schroter, J. A. Krieger, T. Schmitt, V. N. Strocov, S. Pyon, T. Takayama, H. Takagi, O. J. Lipscombe, S. M. Hayden, M. Ishikado, H. Eisaki, T. Neupert, M. Mansson, C. E. Matt, and J. Chang, Phys. Rev. Lett. **121**, 077004 (2018).
[7] J. K. Perry and J. Tahir-Kheli, Phys. Rev. B **58**, 12323 (1998).
[8] N. Ru, C. L. Condron, G. Y. Margulis, K. Y. Shin, J. Laverock, S. B. Dugdale, M. F. Toney, and I. R. Fisher, Phys. Rev. B **77**, 035114 (2008).
[9] V. Brouet, W. L. Yang, X. J. Zhou, Z. Hussain, R. G. Moore, R. He, D. H. Lu, Z. X. Shen, J. Laverock, S. B. Dugdale, N. Ru, and I. R. Fisher, Phys. Rev. B **77**, 235104 (2008).
[10] D. Wu, Q. M. Liu, S. L. Chen, G. Y. Zhong, J. Su, L. Y. Shi, L. Tong, G. Xu, P. Gao, and N. L. Wang, Phys. Rev. Mater. **3**, 024002 (2019).

[11] M. Lavagnini, H.-M. Eiter, L. Tassini, B. Muschler, R. Hackl, R. Monnier, J.-H. Chu, I. R. Fisher, and L. Degiorgi, Phys. Rev. B **81**, 081101(R) (2010).
[12] R. G. Moore, V. Brouet, R. He, D. H. Lu, N. Ru, J.-H. Chu, I. R. Fisher, and Z.-X. Shen, Phys. Rev. B **81**, 073102 (2010).
[13] A. A. Sinchenko, P. Lejay, and P. Monceau, Phys. Rev. B **85**, 241104(R) (2012).
[14] L. J. van der Pauw, Philips Res. Rep. **16**, 187 (1961).
[15] A. A. Sinchenko, P. D. Grigoriev, P. Lejay, and P. Monceau, Phys. Rev. B **96**, 245129 (2017).
[16] See Supplemental Material at http://link.aps.org/supplemental/10.1103/PhysRevB.100.081109 for further information regarding the Hall effect measurements, resistivity, and x-ray diffraction.
[17] A. Girard, T. Nguyen-Thanh, S. M. Souliou, M. Stekiel, W. Morgenroth, L. Paolasini, A. Minelli, D. Gambetti, B. Winkler, and A. Bosak, J. Synchrotron Radiat. **26**, 272 (2019).
[18] Above $T_{\mathrm{CDW1}}$ there are four crossing points, but two of them disappear after the $\mathrm{CDW}_1$ energy gap opens.
[19] F. Schmitt, P. S. Kirchmann, U. Bovensiepen, R. G. Moore, L. Rettig, M. Krenz, J.-H. Chu, N. Ru, L. Perfetti, D. H. Lu, M. Wolf, I. R. Fisher, and Z.-X. Shen, Science **321**, 1649 (2008).
[20] In the second-quantization formalism this Hamiltonian writes down as $\hat{H}_{\boldsymbol{k}} = \epsilon_1(\boldsymbol{k})a_1^{\dagger}(\boldsymbol{k})a_1(\boldsymbol{k}) + \epsilon_2(\boldsymbol{k})a_2^{\dagger}(\boldsymbol{k})a_2(\boldsymbol{k}) + Va_2^{\dagger}(\boldsymbol{k})a_1(\boldsymbol{k}) + V^*a_1^{\dagger}(\boldsymbol{k})a_2(\boldsymbol{k})$.
[21] G. Grüner, *Density Waves in Solids*, 1st ed. (CRC Press, Boca Raton, FL, 2000).
[22] The extra factor 2 comes from the summation over two bands.
[23] B. F. Hu, B. Cheng, R. H. Yuan, T. Dong, and N. L. Wang, Phys. Rev. B **90**, 085105 (2014).
[24] A. A. Sinchenko, P. D. Grigoriev, P. Lejay, and P. Monceau, Phys. Rev. Lett. **112**, 036601 (2014).
[25] M. D. Johannes and I. I. Mazin, Phys. Rev. B **77**, 165135 (2008).
[26] H.-M. Eiter, M. Lavagnini, R. Hackl, E. A. Nowadnick, A. F. Kemper, T. P. Devereaux, J.-H. Chu, J. G. Analytis, I. R. Fisher, and L. Degiorgi, Proc. Natl. Acad. Sci. USA **110**, 64 (2013).
[27] Taking into account the contribution from the gapped parts of the Fermi surface at $|k_x| < k_{x0}$, assuming the mean-field temperature dependence of the $\mathrm{CDW}_1$ energy gap $\Delta_1$, reduces the slope of the $\chi(T)$ dependence by 11% in the interval 95–185 K, increasing the hysteresis range by these 11% to almost 140 K. However, this correction may exceed the accuracy of our model, e.g., of the known electron dispersion and constant *e–e* coupling.